https://dx.doi.org/10.4314/ijs.v26i3.9

SIMULTANEOUS DETECTION OF MULTIPLE COUNTERFEIT BANKNOTES USING RAMAN SPECTROSCOPY: A CASE STUDY OF ₦500 AND ₦1000 NOTES

Ahmed, M. K.* **and Ali, M. H.**

[1]Department of Physics, Faculty of Physical Sciences, College of Natural and Pharmaceutical Sciences, Bayero University, Kano, Nigeria.

*Corresponding Author's Email: shugabamakamban1@gmail.com

(Received: 31st October, 2024; Accepted: 15th November, 2024)

ABSTRACT

A bundle of ₦500 and ₦1000 notes were analyzed using Raman spectroscopy to simultaneously detect and localize multiple counterfeit notes mixed with genuine ones in the bundle. The research applied machine learning techniques, specifically Multiview non-negative matrix factorization (Mv-NMF) and 2D correlation analysis, to detect and assess the spectral similarity between the bundle contents and a reference genuine note, identifying individual spectra as either genuine or counterfeit. Furthermore, an approach was provided for the spatial localization of each sample banknote within a bundle, offering a detailed visualization of all banknotes in the bundle simultaneously. This research showcases the potential of Raman spectroscopy in molecular forensic analysis of a bundle for detecting and identifying the spectral signatures of multiple banknotes with a single banknote's security features, offering a viable alternative to existing individual banknote analysis and detection methods. The research may also be applicable to any security documents with a unique substrate paper that can be bundled together. Our findings offer significant benefits to financial authorities, legal institutions, and intelligence organizations around the world for the smart identification of multiple counterfeited notes.

Keywords: Raman spectroscopy, Naira banknotes, Short edge, Substrate security, Multiple genuine and counterfeit notes, Spatial localization.

INTRODUCTION

Document security, particularly for banknotes, has been a long-standing concern for authorities at various stages, from production to circulation. Here, we are concerned with the circulation stage, where banknotes are distributed in bundles and criminals often sabotage the process by concealing their counterfeit copies. This criminal activity exploits the limitations of our visual system in discriminating between two highly similar colors (Gegenfurtner, 2003) and our sense of touch in differentiating between textures of two similar materials (Cody *et al.*, 2017) as they pass between our fingertips. To further complicate matters, criminals cleverly mix counterfeit notes with authentic ones within a single bundle, making it difficult to identify fake notes when they are in circulation. To counteract this criminal activity, financial institutions use physical examination and specialized scanners in their operations. However, criminals have adapted to technological advancements by producing sophisticated counterfeit notes, such as "super notes" (Takalo *et al.*, 2014), to evade detection. This has led to numerous instances of large-scale counterfeited banknotes (Ali, June 9, 2023; Donatus, December 8, 2023) in various economies worldwide, highlighting the need for innovative solutions to combat this criminal activity.

The most effective methods for detecting high-quality counterfeit banknotes in the current literature typically involve analyzing the chemical composition of the substrate (Marabello, Benzi, Lombardozzi, & Strano, 2017) or ink (Zamalloa, Luízar, & Araujo, 2018) used in banknote production, as mimicking the exact molecular constituents used in authentic notes is challenging. Scientists, therefore, adopt Raman spectroscopy to obtain a unique photonic fingerprint of the constituent molecules of suspected notes to differentiate them from genuine ones. Raman spectroscopy involves photon-molecule interactions with lasers, such as Nd-YAG lasers (1064 nm and 532 nm) and diode lasers (630 and 780 nm) (Ruchita & Agrawal, 2011), resulting in characteristic energy transitions of the molecules that produce a unique photonic fingerprint of those molecules within the material. The useful transitional energy signature E could be either Stokes ($E_s = E_0 - E_u$) and anti-Stokes ($E_{as} = E_0 + E_u$) Raman scattering. Depending on the type and number N of active Raman molecular species involved, the Raman intensity $I_{(u)R}$ varies (Brigitt *et al.*, 2018; Pelletier, 2003).

$$I_{(u)_R} = \frac{16\pi^3}{45.3^2.C^4} \cdot \frac{hI_L N(u_0-u)^4}{\mu u\left(1-e^{hv/kT}\right)} \times [45(\alpha'_a)^2 + (\gamma'_a)^2] \quad 1$$

Where c = Speed of light, h = Planck's constant, π = 3.143, T = Absolute temperature, k = Boltzmann constant, N = Number of scattering active Raman molecules, I_L = Excitation intensity, u = Molecular vibrational frequency in Hertz, u_0 = Laser excitation frequency in Hertz, μ = Reduced mass of the vibrating atoms, ' = Mean value invariant of the polarizability tensor, γ'_α = Anisotropy invariant of the polarizability tensor

Previous studies have used spectral fingerprints of molecules from various cellulose materials, including print paper (He, Bitla, Bousfield, & Tripp, 2002; Workman, 2001), banknotes (Brandão *et al.*, 2016; Guedes *et al.*, 2013; Hana, Pavel & Milan, 2019; Jauković, 2019; Vaskova & Valasek, 2016), driver's licenses (Brandão *et al.*, 2016), cotton (Was-Gubala & Machnowski, 2014), cotton fabric (Luo, Xie & Fan, 2014), and wood (Gierlinger *et al.*, 2010) for sample validation. Typically, a pure Raman spectrum is detected when the material involved has a unique and single Raman-active molecule (Gordon & Mcgoverin, 2011). On the other hand, samples with multiple active Raman molecules will contribute different spectral components, resulting in an overall spectrum that combines the individual spectra of those molecules, forming a single composite Raman spectrum (Brigitta *et al*, 2018; Gordon & Mcgoverin, 2011). When multiple samples are stacked together and analyzed simultaneously, the detected spectrum is a composite of their individual Raman spectra, forming an overall linear mixture of different sample spectra. Additionally, different composite spectra will be detected when a stack of samples is analyzed in different orientations. Although the variation may not be significant when a depolarized Raman spectrum of an isotropic material (e.g., paper) is detected compared to a polarized Raman spectrum of a crystalline material. The composite data of stacked samples detected from different orientations will be complex, containing multiple layers of information that require advanced analysis techniques to reveal valuable insights.

Since the pioneering work by Daniel and Seung's team in 1999, data unmixing techniques, particularly nonnegative matrix factorization (NMF), have proven valuable in many scientific fields (Lee & Choi, 2009; Peter Weiderer, 2019). Depending on the data type, different NMF methods are required for various types of data collected. Consequently, different NMF variants have been proposed in the literature for diverse datasets (Jing, 2017; Yang & Wang, 2018; Yu-Xiong & Yu-Jin, 2013). For example, Multiview NMF is a variant of NMF that seeks semantic features within data generated from multiple orientations of a sample in addition to decomposing the data into two lower ranks.

When banknotes are bundled together, the security features embedded in the substrate material along the longer and shorter edges become the only accessible features common to all notes on the bundle's surface. This unique stacking arrangement enables the simultaneous examination of substrate security features across all banknotes in the bundle and allows for the rapid identification of both genuine and counterfeit notes in a single process. The surfaces consist of molecular components, such as cellulose, hemicellulose, lignin, fillers, and additives (Jerome & Workman, 2001; Kylie, Sarah & Claude, 2013), including titanium dioxide as a crystalline component, unique to each paper type (Bitla, 2002; Marabello, Benzi, Lombardozzi, & Strano, 2017). Furthermore, depending on how the paper note was manufactured (Kylie, Sarah & Claude, 2013), different types of paper may vary in the overall fiber orientation within the sheet (Takalo *et al.*, 2014; Linder & Lofqvist, 2012). Most fibers within a paper are oriented towards the running direction of the paper machine (Linder & Lofqvist, 2012), which is the primary axis of the fibers in the paper (Figure 1), structuring each note into a heterogeneously unique and complex material. This structural combination of components and fiber alignment gives each paper note type distinct properties and characteristics, making each one a unique and complex material.

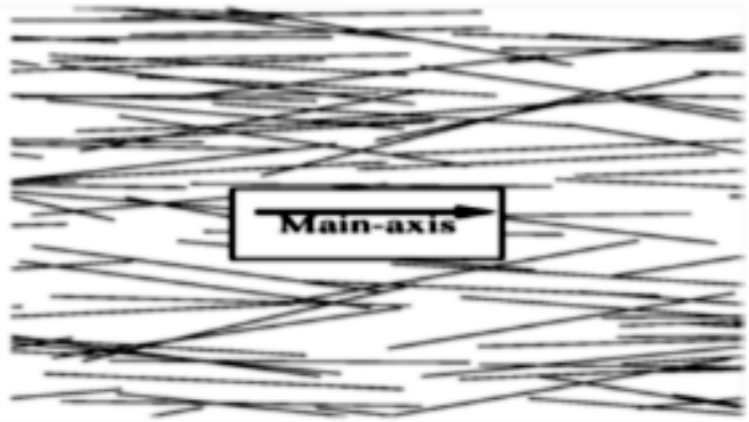

Figure 1. Illustration of fibers alignment in a substrate paper (Linder & Lofqvist, 2012).

In this work, we investigated the applicability of Raman spectroscopy in simultaneous detection of spectra from multiple genuine and counterfeit ₦1000 and ₦500 banknotes on the shorter edge of a bundle, identifing each note's multiview spectra as genuine or counterfeit and established their potential spatial localization within the bundle.

MATERIALS AND METHODS

Sample Preparation

Genuine samples of ₦1000 notes (151 mm x 78 mm) and ₦500 notes (151 mm x 78 mm), along with their counterfeit versions, were collected from bank tellers, automated teller machines (ATM), Bureau de Change, and point-of-sale (POS) operators. A number of unprinted (blank) copies of each denomination were made with A4 commercial print paper (Amazon brand) without any further preparation. To ensure uniformity in the orientation of the substrate's machine direction (MD) along the longer and shorter sides of these homemade blank notes, the shorter and longer sides were cut along the longer and shorter sides of the main A4 paper sheet (i.e., parallel to the shorter and longer sides of the A4 paper sheet), respectively. Similar denominations of the genuine, counterfeit Naira notes, and blank notes were mixed to form each bundle, as shown in Table 1. Each bundle was inserted into a homemade Perspex casing with a small opening (3 mm), exposing the stacked shorter edge (for analysis) of the bundle (Figure 2).

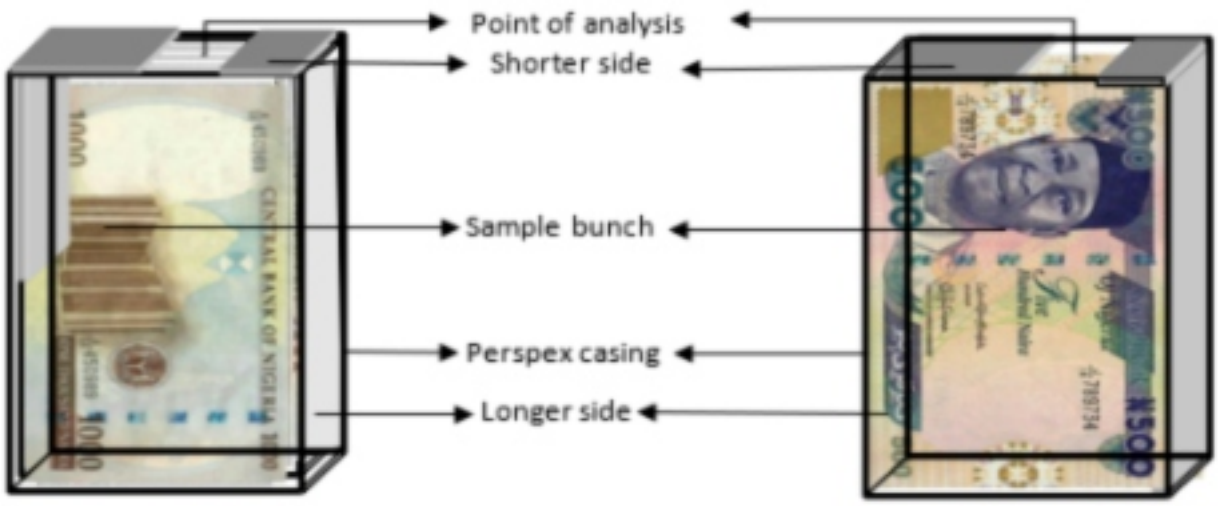

Figure 2. ₦1000 and ₦500 Sample bundles prepared and placed in the Perspex casing with their shorter side showing the point of analysis (all in front view).

Table 1. Description of bundles' content and arrangement.

Sample bundle	Denomination	Blank note content	Counterfeit note content	Genuine note content	Bundle combination arrangement (Blank paper: 0, Counterfeit: o & Genuine: 1)
A	Blank note	36	0	0	00000000000000000000000000000000000000
B	₦1000 note	35	0	1	00000000000000000000000000000000100000
C	₦500 note	34	0	2	00000100000000000000010000000000000000
D	₦1000 note	29	3	4	000oo00000000000010001000000o010000001
E	₦500 note	32	2	2	000000001o00000000010000o000000000000

Experiment

The experiment was conducted with a WITec Alpha 300R Raman spectrometer equipped with WITec Control 5 software, using confocal techniques to focus the excitation laser through a Zeiss EC Epiplan Neofluar DIC 10X / 0.25 (10X magnification, 0.25 numerical aperture) microscope. A laser source with 120 mW power and a wavelength of 532 nm was used. The initial plan for sample setup on the motorized stage and under the microscope objective of the WITec Alpha 300R is shown in Figure 3. However, due to a insufficient gap between the objective and the motorized stage, the sample bundle could not fit beneath the microscope objective, even when arranged along the longer side (Plate 1). To address this issue, the size of the Perspex casing was adjusted by cutting off the excess part along the longer side. The excess part of the sample bundle (not covered by the casing) was temporarily folded and secured with a rubber band across the shorter side. This adjustment allowed the sample to fit under the microscope objective, directing the excitation light (laser) onto the surface at the point of analysis. To prevent damage to the sample, the excitation power was reduced, and the backscattered Raman spectra were detected with a multi-channel detector (390 x 2600 pixels), recording a full Raman spectrum in 20 accumulations over 0.5 seconds. Multiple views of the sample spectral data were recorded in each rotational position setting (between 0 and 180 degrees in 45-degree intervals). The built-in WITec algorithm, Shape 100, was used to remove cosmic rays, background spectra, and to smooth the spectra. Some fluorescence (photoluminescent) effects were still observed in certain spectral views, so a third-order polynomial was applied to eliminate background fluorescence effects. This same procedure was also used to record all Multiview spectra of the shorter edge of a single-genuine ₦1000 and ₦500 note as reference Multiview spectral data. Additionally, spectra of the Perspex casing edge were recorded. Both spectral graphs and data text were recorded between 57 and 3735 cm^{-1} for analysis.

Data Formation and Preprocessing

The diverse spectral views acquired from each bundle were structured into a single spectral data matrix by concatenating the spectral data views row-wise, with each column containing the spectral intensity evolution across views over the range of 57–3735 cm^{-1} and the rows representing the intensity records for each view, forming 5 x 1695 matrix. However, the composite spectra were expected to include Multiview contributions from the Perspex spectra of the two edges of the casing (Figure 3b) enclosing the bundle. These spectra were subtracted from the Multiview composite data matrix to obtain a pure composite data matrix representing the bundle's Multiview spectral data.

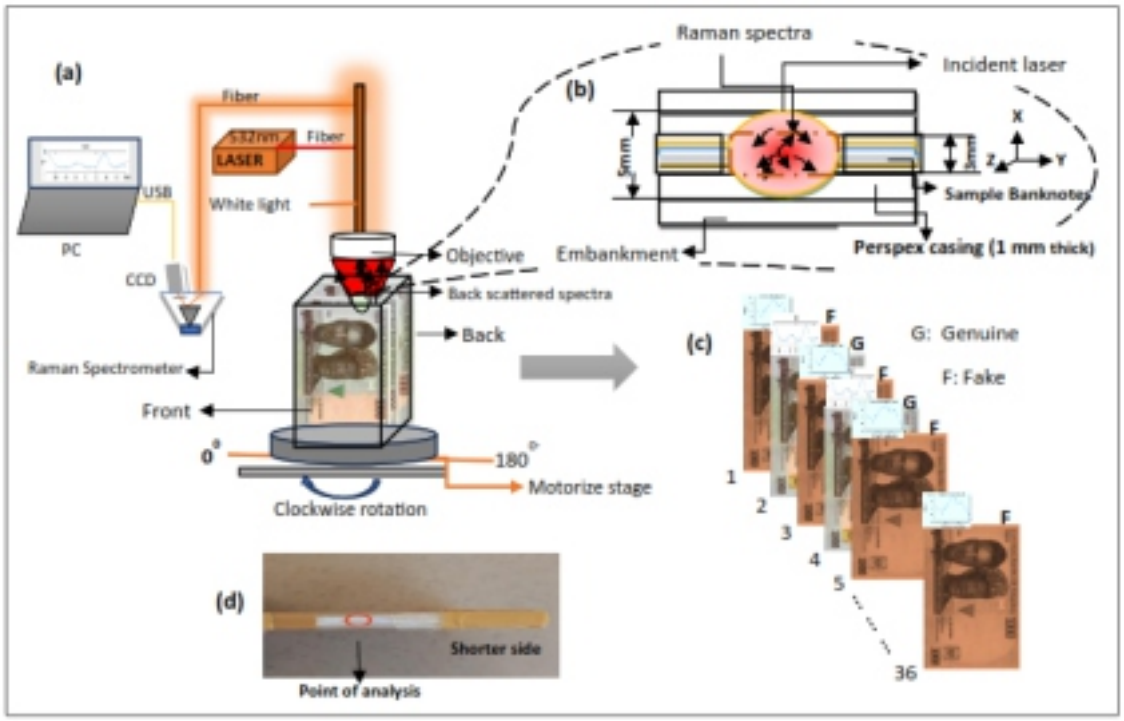

Figure 3. a) Experimental arrangement of the rotational acquisition scheme used in the detection of each composite spectrum of a bundle. b) Point of analysis surface view. c) Decomposition structure. d) Point of analysis on the Perspex casing.

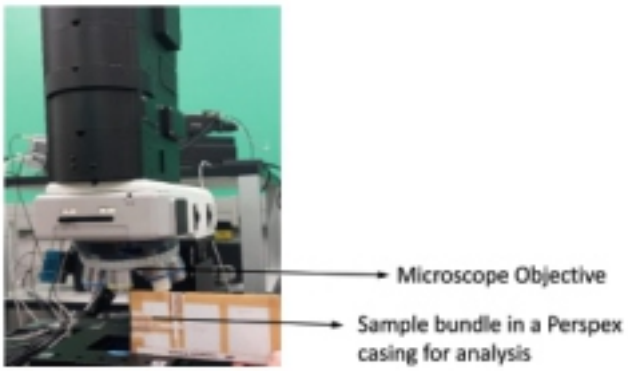

Plate 1. Sample bunch unfit to be set beneath the WITEC Alpha 300R microscope objective even in the longer side setting arrangement. **Credit**: Electron Microscope Unit, University of Cape Town, Rondebosch, 7700 South Africa.

MODEL FORMULATION

The composite Raman spectra detected by the charge-coupled device (CCD) from various sample bunch orientations represent a combination of dominant spectral contributions from each sample note in the bunch. These spectra reveal the unique overall vibrational modes of active Raman molecules within the substrate of individual banknotes, along with their respective concentrations. The component spectra contribution of individual banknotes is an overall representation of the source molecules' spectra within the substrate of a particular banknote. Depending on the Raman-active molecules in the fiber and coatings of the substrate note relative to the linearly polarized laser plane of orientation, the depolarized composite spectrum detected will vary with each rotational orientation, although significant variations are not expected, especially because paper substrates are typically isotropic materials and the detected spectra are of the depolarized type.

To generate a data matrix for each sample bunch, recorded composite Raman spectra at different angular rotational points $\theta_1 \ldots . \theta_M$ (v = views) within K wavenumber range are concatenated row-wise to form M x K data matrix. This approach provides insights into how the overall spectral composition of the entire sample bunch changes as the rotational angle is adjusted. Therefore, given a nonnegative data matrix $\boldsymbol{D} = [d_1, d_2 d_3, \ldots\ldots\ldots d_K] \in \mathbb{R}^{M \times K}$, NMF aims to approximate $\boldsymbol{D}$ into two lower-rank matrices: a Multiview basis matrix $\boldsymbol{A} \in \mathbb{R}^{M \times N}$ and a coefficient matrix $\boldsymbol{S} \in \mathbb{R}^{K \times N}$ with an error matrix $\boldsymbol{E} \in \mathbb{R}^{M \times K}$, approximating the original data as

$$\boldsymbol{D} = \boldsymbol{A}\boldsymbol{S}^T + \boldsymbol{E} \qquad 2$$

The two matrices factors in equation 2 are (Miron, Dossot, Carteret, Margueron, & Brie, 2011)

$$\boldsymbol{A} = \begin{pmatrix} i_1^{(v)}(\theta_1) \ldots i_N^{(v)}(\theta_1) \\ \cdot \quad \ldots \quad \cdot \\ i_1^{(v)}(\theta_M) \ldots i_N^{(v)}(\theta_M) \end{pmatrix} \in \mathbb{R}^{M \times N} \qquad 3$$

$$\boldsymbol{S} = \begin{pmatrix} s_1^{(v)}{}_{,(\lambda_1)} \ldots s_N^{(v)}{}_{,(\lambda_1)} \\ \cdot \quad \ldots \quad \cdot \\ s_1^{(v)}{}_{,(\lambda_K)} \ldots s_N^{(v)}{}_{,(\lambda_K)} \end{pmatrix} \in \mathbb{R}^{K \times N} \qquad 4$$

Equations 3 and 4 were modified for the Multiview depolarize data that was detected in this work.

Each column entry of the basis matrix (Equation 3) corresponds to the overall spectral intensity of an individual sample note at different rotational angles for a particular wavenumber. These entries provide a measure of how the spectral characteristics of each sample note vary with changes in the rotational angle. On the other hand, the row intensity entries in the same equation represent the collective spectral intensity contributions of all sample notes within the bunch, each assessed at a specific rotational angle. For the coefficient matrix (Equation 4), the columns and rows correspond to the spectral coefficients of the columns and rows of the matrix in Equation 2, respectively. The rows of the coefficient matrix align with those in Equation 3, representing the spectral coefficients for the overall spectral intensity contributions of each sample note within the bunch at specific rotational angles. In simpler terms, the coefficient matrix essentially shows how various spectral components are weighted or combined to form the observed data spectra for each sample note on each rotational angle.

Multiview objective function formulation

To solve Equation (2) using the NMF minimization problem, we first derive the objective function by applying the Frobenius norm, which minimizes the error in the estimate,

$$\|\boldsymbol{E}\|_F^2 = \|\boldsymbol{D} - \boldsymbol{A}\boldsymbol{S}^T\|_F^2 \qquad 5$$

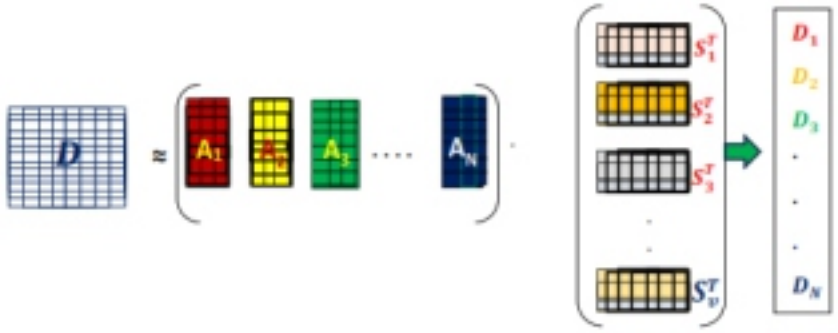

Figure 4. A Schematic illustration of composite data matrix $\boldsymbol{D}$ factorize into $\boldsymbol{N}$ basis matrices $\boldsymbol{A}_N$ with column $\boldsymbol{A}_1$ to $\boldsymbol{A}_N$ and the corresponding coefficient matrices (transposed) $\boldsymbol{S}^T$ with $\boldsymbol{S}_1^T$ to $\boldsymbol{S}_v^T$ rows. Their matrix product (linear combination) gives each Multiview spectral data matrices $\boldsymbol{D}_1$ to $\boldsymbol{D}_N$ for sample banknotes in the bunch.

subject to $D, A, S \geq 0$ to nonnegative constraints that must be satisfied in the minimization problem of Equation 2, where $\|.\|_F^2$ is a square Frobenius norm. Generally, the rank of matrices **A**, and **S** is much lower than the rank of D, i.e., $N \ll min\,(M,K)$ where $M < K$.

Equation 5 represents a standard objective function that can structure the data matrix into a homogeneous single data spectral view, disregarding the inherent Multiview semantic features present in the collected data (Wang *et al.*, 2012). To explore the diverse spectral feature

views expected in each banknote's Multiview spectra result, we introduce a Multiview diversity constraint, $\sum_{w=1,w\neq v}^{V} tr\left(\boldsymbol{S}^{(v)}\boldsymbol{S}^{(w)^T}\right)$.
This constraint ensures that any two data vectors are orthogonal to each other, each column vector of matrix $\boldsymbol{S}$ is orthogonal to the others, thereby enforcing component diversity of different views. This orthogonality is achieved when the product of the vectors is approximately zero (Jing, 2017). To guarantee the diversity of any two pairs of different spectral view *v view* and *w view*, we enforce the proposed diversity constrain. Therefore, the Multiview objective function is:

$$\underset{s.t\ \boldsymbol{D}^{(v)},\boldsymbol{A}^{(v)},\boldsymbol{A}^{(w)},\boldsymbol{S}^{(v)},\boldsymbol{\alpha},\boldsymbol{\beta}\geq 0}{minimize}$$
$$\sum_{v=1}^{V}\left\|\boldsymbol{D}^{(v)}-\boldsymbol{A}^{(v)}\boldsymbol{S}^{(v)^T}\right\|_F^2+\boldsymbol{\alpha}\left\|\boldsymbol{S}^{(v)}\right\|_F^2$$
$$+\beta\sum_{w=1,w\neq v}^{V} tr\left(\boldsymbol{S}^{(v)}\boldsymbol{S}^{(w)^T}\right) \quad 6$$

Where the first and second terms are rank approximation terms, and & β are regularization parameters that ensure smooth balance between the parameter terms and the errors as well (Cheng *et al.*, 2010; Tian & Zhang, 2022). This equation is further expanded to:

$$tr\left(\boldsymbol{D}^{(v)}\boldsymbol{D}^{(v)^T}-2\boldsymbol{D}^{(v)}\left(\boldsymbol{S}^{(v)}\boldsymbol{A}^{(v)^T}\right)+\left(\boldsymbol{A}^{(v)}\boldsymbol{S}^{(v)^T}\right)\left(\boldsymbol{S}^{(v)}\boldsymbol{A}^{(v)^T}\right)\right)$$
$$+\ \boldsymbol{\alpha}\,tr\left(\boldsymbol{S}^{(v)}\boldsymbol{S}^{(v)^T}\right)+\beta\sum_{w=1,w\neq v}^{V} tr\left(\boldsymbol{S}^{(v)}\boldsymbol{S}^{(w)^T}\right) \quad 7$$

Optimization Problem

For the Multiview objective function (Equation 6) to converge to a local minimum to have a global minimum, it should be convex on both $\boldsymbol{A}^{(v)}$ and $\boldsymbol{S}^{(v)}$ variables simultaneously. Therefore, we use algorithm to find the local minima that can iteratively update $\boldsymbol{A}^{(v)}$ keeping $\boldsymbol{S}^{(v)}$ fix, follow by updating $\boldsymbol{S}^{(v)}$ with $\boldsymbol{A}^{(v)}$ fix.

For the minimization procedure, we find the Lagrange function $\mathcal{L}\left(\boldsymbol{A}^{(v)},\boldsymbol{S}^{(v)}\right)$ of Equation 6, and by letting $\omega_{pq}^{(v)}$ *and* $\delta_{pq}^{(v)}$ to be respective Lagrange multipliers that $\omega^{(v)}=[\omega_{pq}^{(v)}]$ and $\delta^{(v)}=[\delta_{pq}^{(v)}]$ for a constrain $\left[i_N^{(v)}(\theta_M)\right]_{pq}\geq 0$ and $\left[s_N^{(v)}{}_{(\lambda_K)}\right]_{pq}\geq 0$

variables in the nonnegative problem of Equation 6. Equation 7 can be solved by taking the matrix differentiation (Pedersen, 2012) with respect to $\boldsymbol{A}^{(v)}$ keeping $\boldsymbol{S}^{(v)}$ fix and then $\boldsymbol{S}^{(v)}$ letting $\boldsymbol{A}^{(v)}$ fix. At a local minimum both equate to zero. Applying Karush-Kuhn-Tucker (KKT) condition (Boyd & Vandenberghe, 2006) for the nonnegativity on $\boldsymbol{A}^{(v)}$ and $\boldsymbol{S}^{(v)}$, the update rule for the basis matrix $\boldsymbol{A}^{(v)}$ and coefficient matrix $\boldsymbol{S}^{(v)}$ of Equation 6 are:

$$(\boldsymbol{A})_{pq}^{(v)}\leftarrow(\boldsymbol{A})_{pq}^{(v)}\odot\frac{\left((\boldsymbol{D})^{(v)}((\boldsymbol{S})^{(v)})\right)_{pq}}{\left((\boldsymbol{A})^{(v)}(\boldsymbol{S})^{(v)^T}((\boldsymbol{S})^{(v)})\right)_{pq}} \quad 8$$

For the coefficient matrix $\boldsymbol{S}^{(v)}$ of the views

$$(\boldsymbol{S})^{(v)}{}_{pq}\leftarrow(\boldsymbol{S})^{(v)}{}_{pq}\odot$$
$$\frac{\left(2(\boldsymbol{D})^{(v)^T}(\boldsymbol{A})^{(v)}\right)_{pq}}{\left(2\left((\boldsymbol{S})^{(v)}(\boldsymbol{A})^{(v)^T}\right)(\boldsymbol{A})^{(v)}+2\,\boldsymbol{\alpha}(\boldsymbol{S})^{(v)}+\beta\sum_{w=1,w\neq v}^{V}(\boldsymbol{S})^{(w)}\right)_{pq}} \quad 9$$

where $\odot$ and $\div$ is element wise multiplication and element wise division respectively.

Spectral similarity metrics of Genuine ₦1000/₦500 note and bundle content

To identify a genuine note in a bundle content we employ a multi-step approach. First, the spectral data of the reference genuine banknote (₦1000 or ₦500) $\boldsymbol{A}_b$ obtained, serves as a benchmark for comparison. Next, the similarity between the reference genuine banknote and each multiview spectra $\boldsymbol{B}_{Cn}$ sets of each bundle's content are evaluated by calculating both vertical correlations $\boldsymbol{r}_v$ and horizontal correlations $\boldsymbol{r}_h$ given in Equations 10 and 11, as described by Dikbaş (2017). These provide a quantitative measure of the similarity between the spectral features of the reference note and each individual note in the bundle. Vertical correlations assess the similarity in intensity averages across views, while horizontal correlations examine the similarity in intensity averages among view sets. By employing this approach, a detailed understanding of the similarity between the reference genuine banknote and each individual note in the bundle can be obtained in the two-dimensions.

$$\boldsymbol{r}_h=\frac{\sum_M\sum_N\left(\boldsymbol{A}_{b\,MN}-\overline{\boldsymbol{A}_{b\,M}}\right)\left(\boldsymbol{B}_{C_{n\,MN}}-\overline{\boldsymbol{B}_{C_{n\,M}}}\right)}{\sqrt{\left[\sum_M\sum_N\left(\boldsymbol{A}_{b\,MN}-\overline{\boldsymbol{A}_{b\,M}}\right)^2\right]\left[\sum_M\sum_N\left(\boldsymbol{B}_{C_{n\,MN}}-\overline{\boldsymbol{B}_{C_{n\,M}}}\right)^2\right]}} \quad 10$$

$$\boldsymbol{r}_v=\frac{\sum_M\sum_N\left(\boldsymbol{A}_{b\,MN}-\overline{\boldsymbol{A}_{b\,N}}\right)\left(\boldsymbol{B}_{C_{n\,MN}}-\overline{\boldsymbol{B}_{C_{n\,N}}}\right)}{\sqrt{\left[\sum_M\sum_N\left(\boldsymbol{A}_{b\,MN}-\overline{\boldsymbol{A}_{b\,N}}\right)^2\right]\left[\sum_M\sum_N\boldsymbol{B}_{C_{n\,MN}}-\overline{\boldsymbol{B}_{C_{n\,N}}}^2\right]}} \quad 11$$

where $\overline{\boldsymbol{A}_{b\,M}}$, $\overline{\boldsymbol{B}_{C_{n\,M}}}$ and $\overline{\boldsymbol{A}_{b\,N}}$, $\overline{\boldsymbol{B}_{C_{n\,N}}}$ are the averages of Mth row and Nth column of matrix $\boldsymbol{A}_b$ and $\boldsymbol{B}_{cn}$ respectively.

Algorithm

The algorithm is evaluated using MATLAB code generated according to stages provided in Table 2 .

Table 2. ALGORITHM

1: INPUT; Data matrix $\boldsymbol{D} = [\boldsymbol{d_1}, \ldots \ldots \boldsymbol{d_N}]^{\boldsymbol{T}}$, reference genuine note data matrix (₦1000/₦500), $\boldsymbol{N}, \boldsymbol{v}$ **(number of views)**, maximum number of iterations, $\boldsymbol{\alpha}$ and $\boldsymbol{\beta}$, tolerance

Initialization:

2. Initialize and obtain the Multiview NICA initialization of the basis ($\boldsymbol{A^{(v)}}$) and coefficient ($\boldsymbol{S^{(v)}}$) matrix

3: Retrieve the spectral data matrix for each sample banknote in the bundle based on the result from step 2

Correlation and threshold evaluation:

4: Calculate the vertical and horizontal correlation for each individual initialized spectral sets using equation 10 &11

5. Round each correlation (correlation > 0.5 = 0 for fake note, else = 1 for genuine note) to identify first category of fake and genuine notes in the bundle

6. Use a dynamic threshold (equation 14) to further filter out weaker matches and identify notes spectra with strong similarity to genuine note (equation 12)

Multiview optimization:

7: For $v = 1$ *to* 5 *and* $w = 1$ *to* 5, $v \neq w$ do

8: Use the initialized results in the line 2 to update:

a. Basis matrix $\boldsymbol{A^{(v)}}$ using equation 8

b. Coefficient matrix $\boldsymbol{S^{(v)}}$ using equation 9

For each note in the bundle until convergence or maximum iteration is attained:

9: Get the spectral data matrix for each sample banknote in the bunch from the result in line 8a & b

10. Evaluate stage 4, 5 and 6 for the Multiview optimization results in line 9

11: OUTPUT results: Genuine and counterfeit, and their permutation localization arrangement in the bundle

Product of Permutation with Repetition

The analyzed bundles can be set in either front or back views, leading to dual spatial localization possibilities for each note within the bundle. This phenomenon can be observed by positioning the sample on the motorized stage in both back and front views, resulting in distinct spatial localization indices for the notes in the bundle, depending on the chosen view setting. However, when sample notes are symmetrically arranged within the bundle, their permutation indices remain symmetrical regardless of the view, yielding two possible symmetrical spatial localization indices for identical notes. Consequently, two distinct composite data matrices can be generated for each sample bundle based on the two possible view settings. In our experiment, the front view setting was used for each sample bundle, and the corresponding arrangements are detailed in Table 1, based on the front view count. A procedure for evaluating a product of permutation with repetition that rearranges the entries of the outer permutation (group permutation on the left) is presented in Table 3. Two hypothetical bundle permutations with repetition are presented, each arranged in different permutations. A fix Index (raw two), count from 1 to 6 were assigned to each element of the first permutation group after arranging the elements in ascending order (Shahdan, 1961).

Table 3. Demonstration of permutation product with repetition of two hypothetical bundle with 6 samples

S/No	Rows description	Outer Permutation	Inner Permutation	Permutation Product
1	**Count**	$\begin{pmatrix}1&2&3&4&5&6\end{pmatrix}$	$\begin{pmatrix}1&2&3&4&5&6\end{pmatrix}$	$\begin{pmatrix}1&2&3&4&5&6\end{pmatrix}$
	Fix indices	$\begin{pmatrix}4&1&5&6&2&3\end{pmatrix}$	$\begin{pmatrix}4&5&1&2&3&6\end{pmatrix}$	$\begin{pmatrix}6&2&4&1&5&3\end{pmatrix}$
	Group permutation	$\begin{pmatrix}\mathbf{1}&\mathbf{0}&\mathbf{1}&\mathbf{1}&\mathbf{0}&\mathbf{0}\end{pmatrix}$	$\begin{pmatrix}\mathbf{1}&\mathbf{1}&\mathbf{0}&\mathbf{0}&\mathbf{0}&\mathbf{1}\end{pmatrix}$	$\begin{pmatrix}\mathbf{1}&\mathbf{0}&\mathbf{1}&\mathbf{0}&\mathbf{1}&\mathbf{0}\end{pmatrix}$
2	**Count**	$\begin{pmatrix}1&2&3&4&5&6\end{pmatrix}$	$\begin{pmatrix}1&2&3&4&5&6\end{pmatrix}$	$\begin{pmatrix}1&2&3&4&5&6\end{pmatrix}$
	Fix indices	$\begin{pmatrix}1&4&5&2&3&6\end{pmatrix}$	$\begin{pmatrix}3&1&4&2&5&6\end{pmatrix}$	$\begin{pmatrix}5&1&2&4&3&6\end{pmatrix}$
	Group permutation	$\begin{pmatrix}\mathbf{0}&\mathbf{1}&\mathbf{1}&\mathbf{0}&\mathbf{0}&\mathbf{1}\end{pmatrix}$	$\begin{pmatrix}\mathbf{1}&\mathbf{0}&\mathbf{1}&\mathbf{0}&\mathbf{1}&\mathbf{1}\end{pmatrix}$	$\begin{pmatrix}\mathbf{1}&\mathbf{0}&\mathbf{0}&\mathbf{1}&\mathbf{0}&\mathbf{1}\end{pmatrix}$

RESULTS AND DISCUSSION

A comprehensive analysis was conducted on the Multiview composite Raman spectra of five bundles, each containing 36 notes. Specifically, the results for bundles A and B show strong photoluminescence interference (Figures 5a and 5b). Previous research has reported that Raman spectroscopy analysis of paper substrates is often influenced by fluorescence interferences (Brandão *et al.*, 2016; Jauković, 2019; Murtala & Mutari, 2024), and this effect is associated with the surface roughness of some papers such as counterfeit paper (Brandão *et al.*, 2016). In this case, the experiment should be repeated by swapping to the other shorter side of the bundle.

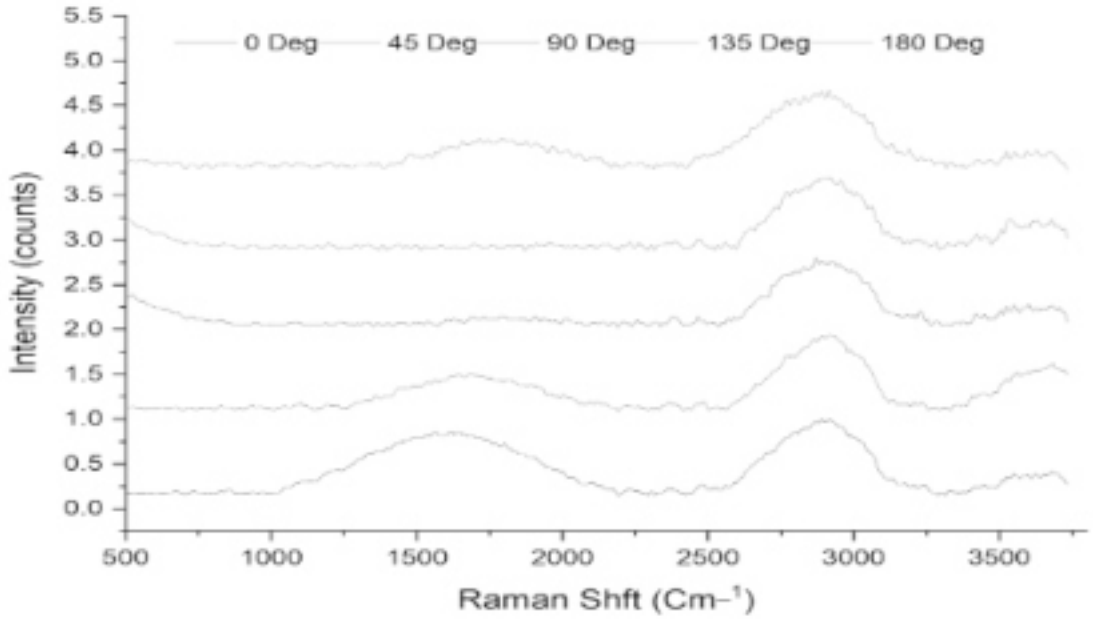

Figure 5a. Bundle A composite Mv spectra set.

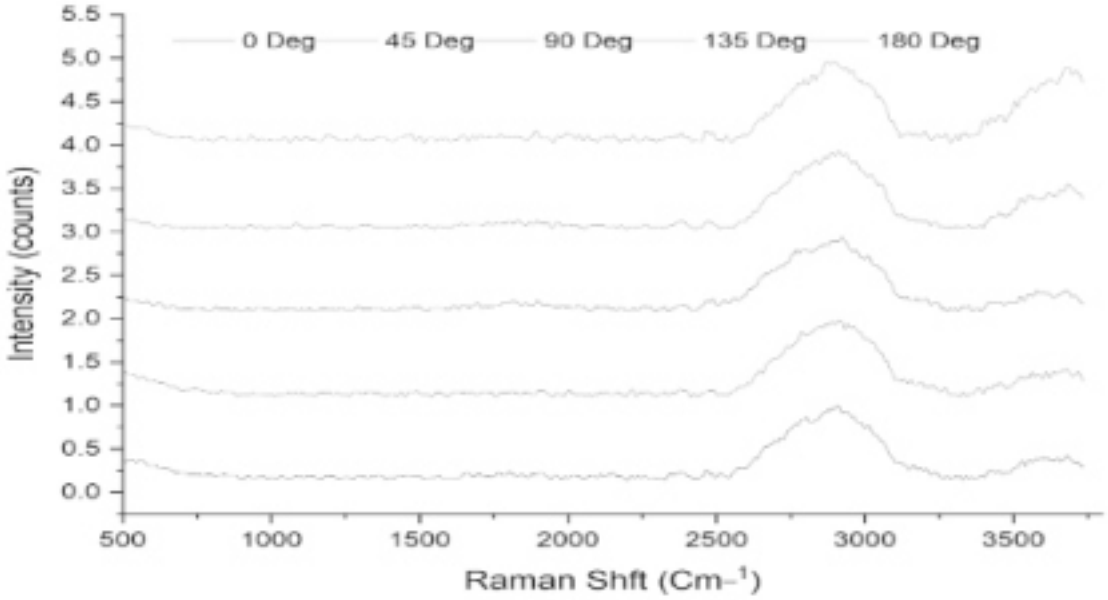

Figure 5b. Bundle B composite Mv spectra set.

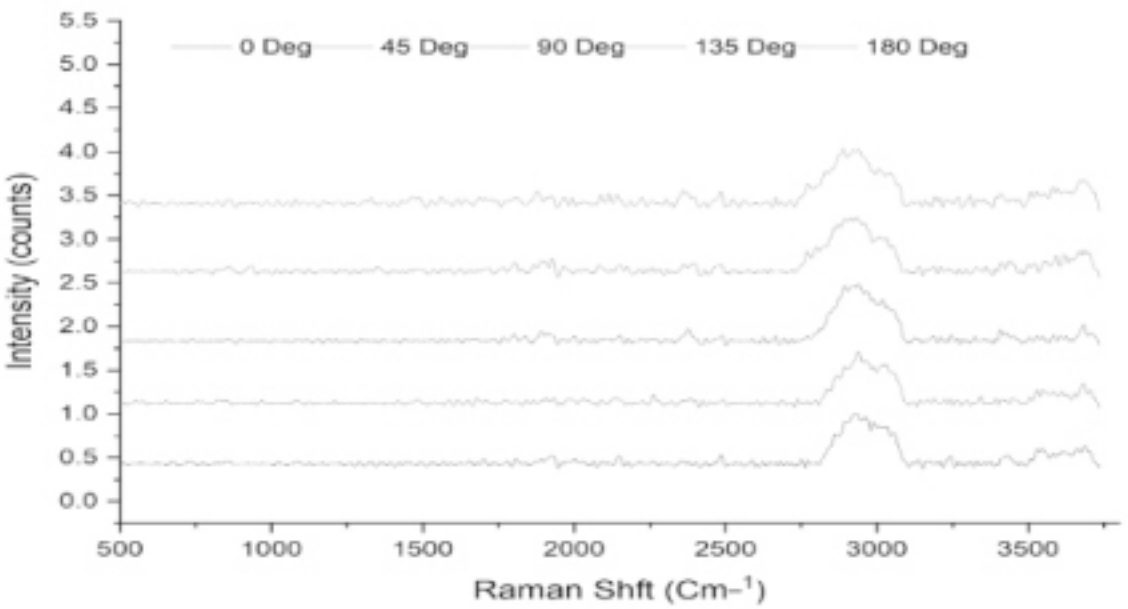

Figure 5c. Bundle C composite Mv spectra set.

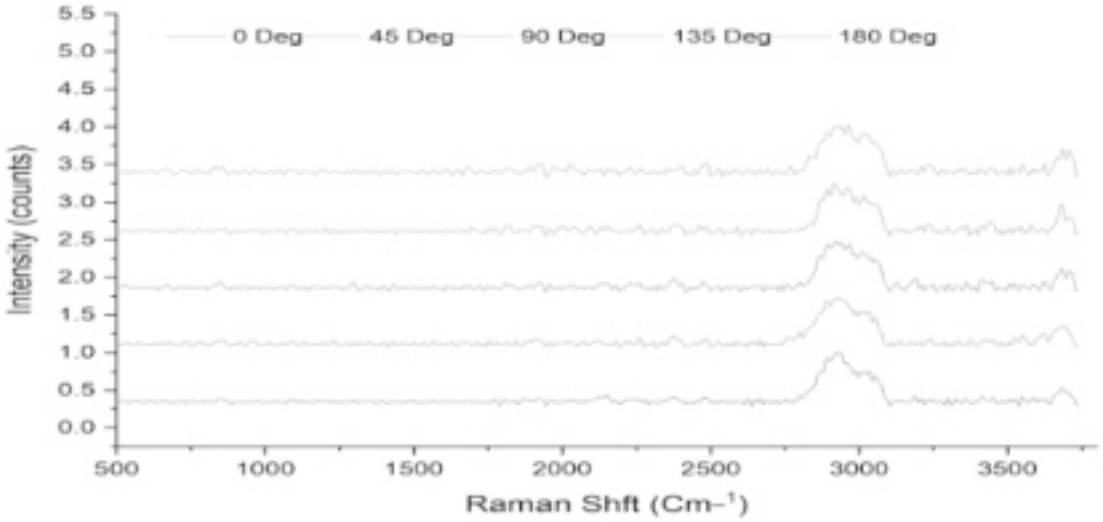

Figure 5d. Bundle D composite Mv spectra set.

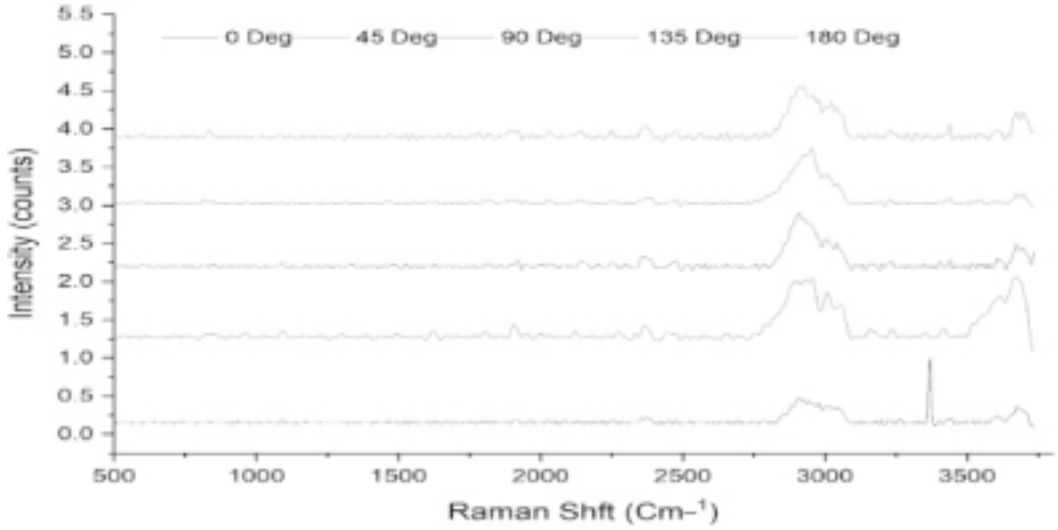

Figure 5e. Bundle C composite Mv spectra set.

The overall composite spectra of bundles C, D, and E revealed minimal diversity in intensity and peak patterns across the different bundles (Figures 5c-e). This is attributed to the similarity of the main constituent molecule (cellulose) across all samples in the bundles, the isotropic nature of the sample notes in each bundle, and the depolarized spectra detected from the samples. While Raman intensities varied slightly across views, the spectral profiles remained consistent. The five composite spectral view sets obtained from bundle E (Figure 5e) also exhibited minimal intensity variation and peak positions across different views, with three exceptions: at 3400 cm^{-1} in view 1, 3450 cm^{-1} in view 5, and above 3500 cm^{-1} in view 2. These shifts, attributed to O–H and N-H stretching from sebum components such as free fatty acids and triglycerides, reflect contamination of banknotes from skin contact. Variations in these regions likely result from differing bonding environments, oxidation, or the thickness of sebum deposits commonly found on handled banknote surfaces (Lawandy, 2014).

Bundles Multiview Spectral Content

The extracted Multiview spectral data sets for the 36 samples of bundles C, D and E were visualized using heatmaps, as shown in Figure 6a-c, to explore the intensity variations across different Raman shifts and views. Each heatmap corresponds to an individual sample's Multiview spectral signature set, with rows representing the five different views and columns representing the Raman shift across the spectral range. The warmer colors (red) indicate higher Raman intensities, and the cooler colors (blue) represent lower Raman intensities. The spectral arrangement (sp1–sp36) was based on the spectral set arrangement of the Multiview decomposition results. This arrangement order will be discussed further and analyzed in the next section for a possible identification of each note's spatial localization in the actual bundle arrangement (Table 1).

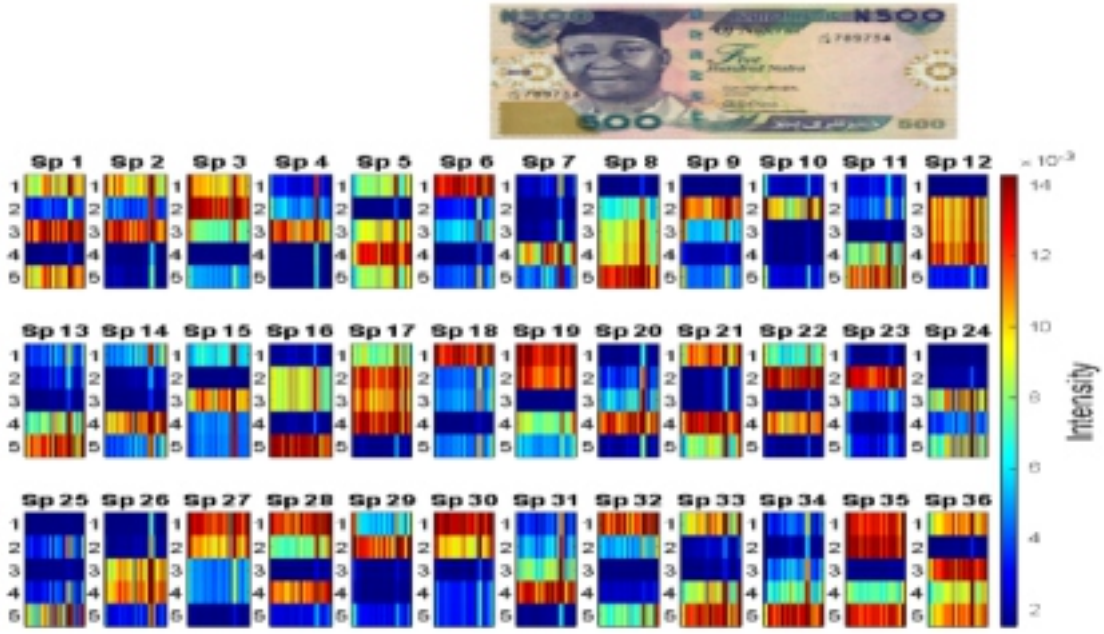

Figure 6a. Heatmaps of Multiview spectral set of samples notes in bundle C.

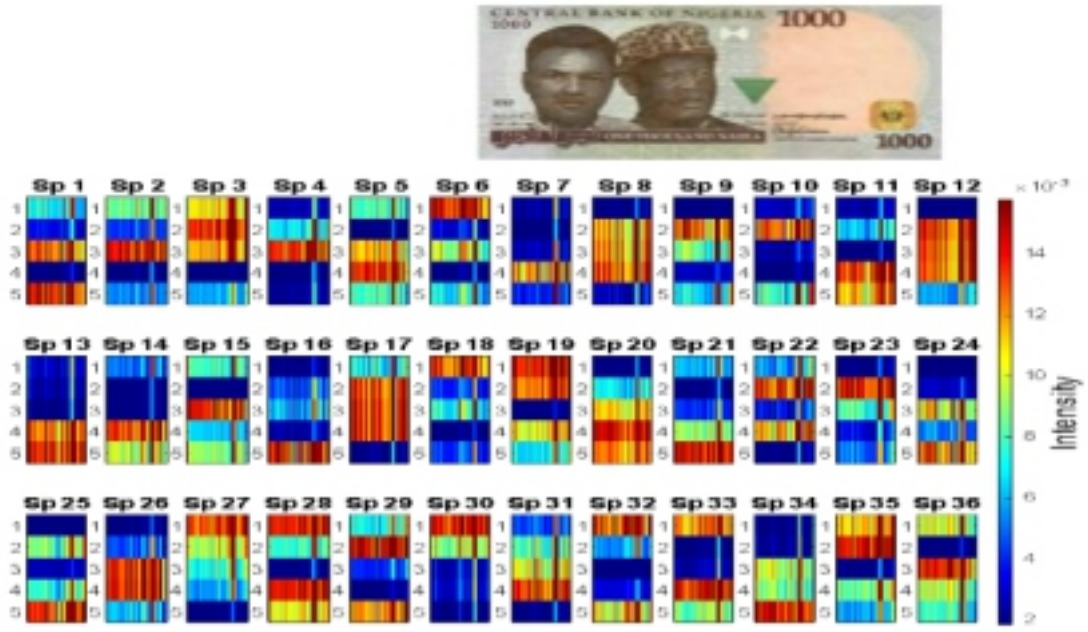

Figure 6b. Heatmaps of Multiview spectral set of samples notes in bundle D.

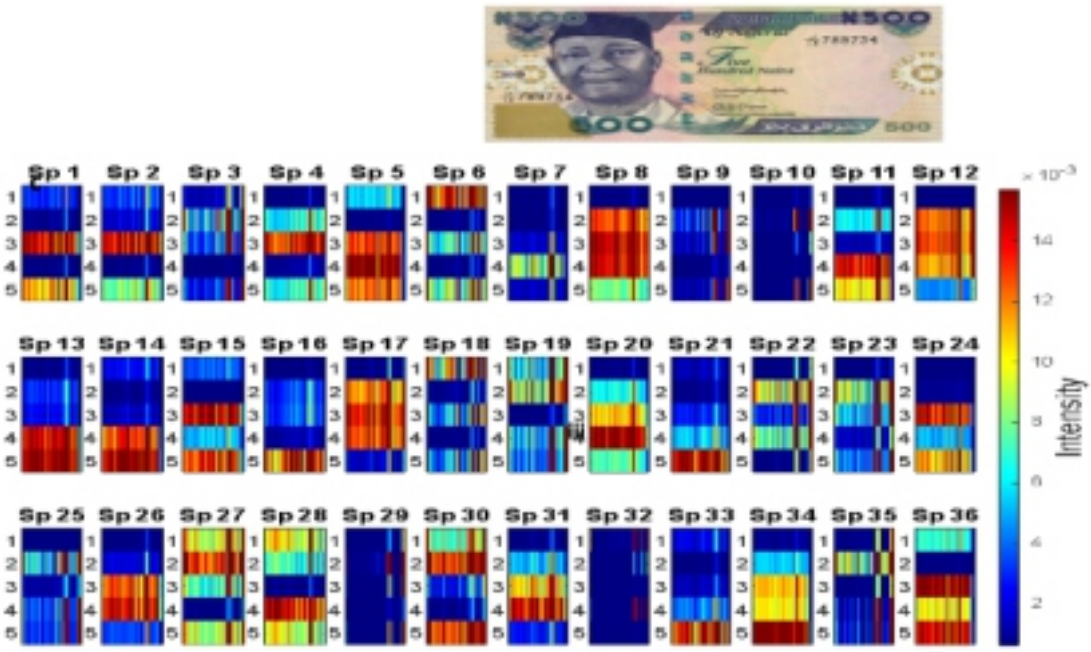

Figure 6c. Heatmaps of Multiview spectral set of samples notes in bundle E.

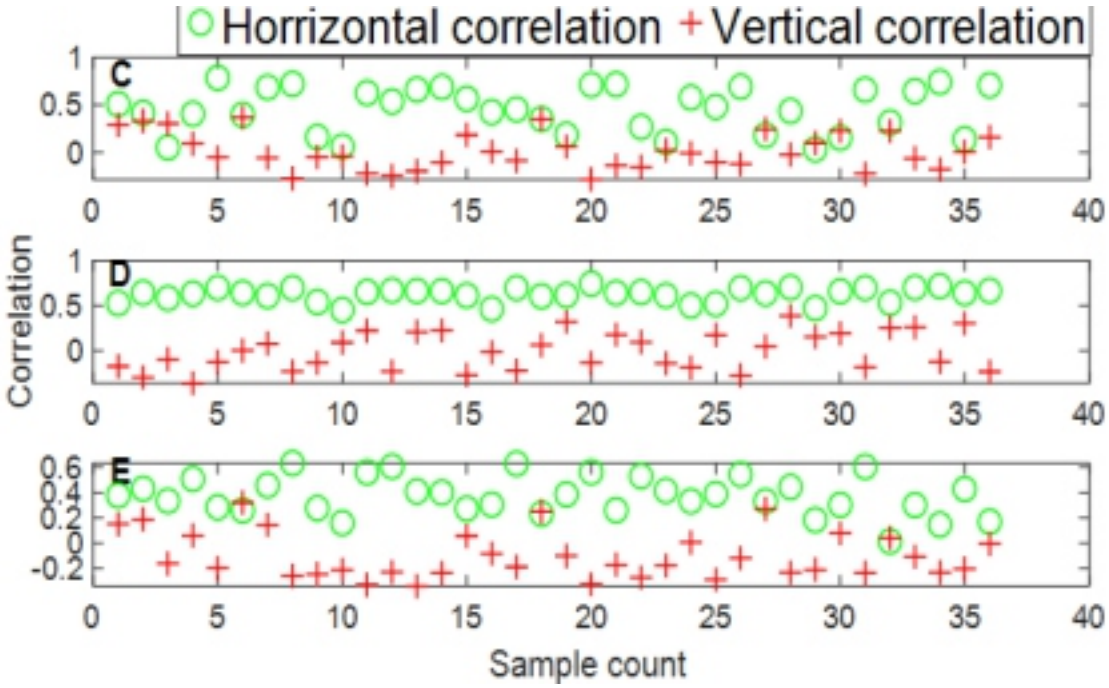

Figure 6d. Horizontal and vertical correlations of each note's spectra in each bundle with the reference genuine note spectra.

All samples displayed subtle spectral intensity variations when compared to other sets. However, some show spectral similarity across views (e.g., sp1 & sp2, sp20 & sp31 in Figure 6(a), sp1 & sp2 in Figure 6(b), and sp1 & sp2 in Figure 6(c). The similar spectral sets likely originate from notes with similar molecular spectral signatures. One noticeable observation in the results was the strong Raman signal spanning between 2800 - 3100 cm^{-1} across all five views. These signal stretches are mostly attributed to C-H stretching modes of cellulose (Agarwal, 2019; James & Rajai, 1987), which occur when the electric vector of the incident light is aligned perpendicularly to the CH bonds relative to the chain axis (James & Rajai, 1987). The overall spectral profile of all extracted spectra (heatmap) shows some commonality among the spectral sets of all bundles (Figure 6a - c). This observation suggests that all notes share a similar material composition, which is reflected in their spectral signatures. This shared feature is attributed to the presence of cellulose molecules (derived from wood and cotton) as a dominant constituent in both samples' notes (Sonnex *et al.*, 2014), which significantly contributes to this similarity. Despite this shared cellulose content, genuine notes are expected to have distinct spectral features arising from specialized molecules in the coatings of their substrate, crystallinity differences in cellulose from wood and cotton (Agarwal, 2019; James & Rajai, 1987; Jerome & Workman, 2001), and certain production processes (Jones, Benson, & Roux, 2013; Takalo *et al.*, 2014; Linder & Lofqvist, 2012) that may distinguish the Multiview spectral signature of genuine notes from counterfeit ones.

Two-Dimensional Correlation Analysis

Since the decomposed Multiview spectral results obtained in the previous section cannot be directly used to identify individual samples in the bundle as genuine or fake notes (counterfeit or blank notes), a 2D correlation analysis (Equations 10 & 11) was conducted to assess the Multiview spectral similarities between each of the NICA-initialized spectra and optimized Multiview spectra of bundle contents (see Section 3.2 and Table 2) with the reference Multiview spectra set of the corresponding genuine Naira note. The 2D similarity assessment compares the averages of spectral intensities in the view sets (horizontal-wise) in each note with that of the reference genuine note. Vertical correlation assesses similarity between the average intensities sets across multiple views (5 views) of each note spectral set and those of the genuine note. The results reveal a range of Multiview spectral and intensity similarities with correlation values

between -1 and 1; some samples display strong (≥ 0.5) correlation, while others show weak (<0.5) correlation with the reference genuine Naira note spectra set. Surprisingly, all bundles show weaker correlation (<0.5) in the vertical direction (Figure 6(d)). Therefore, we did not assess sample similarities in the vertical direction.

Correlation results in the horizontal direction show that none of the samples are inversely (<0) correlated (Figure 6(d)) with the reference genuine note, suggesting that although the spectra of fake notes may be weakly correlated with the reference genuine note, they still share some commonality in the photonic signature of their source molecules. Other Multiview spectral signatures, however, indicate stronger correlation (≥ 0.5) with the corresponding genuine note signature. None of the sample spectra indicate exact similarity (=1) with the genuine note, likely due to error ***E*** associated with the Mv-NMF decomposition procedure for individual composite spectra, as seen in Equation 2.

Bundles content Identification Base on Horizontal Correlation

Based on the preceding correlation results, samples with high correlation values (≥ 0.5) in the horizontal direction are likely candidates for genuine note spectra within the bundle, while those with lower correlation values (<0.5) are considered as fake note spectra. Following this criterion, we transformed weaker and stronger correlation results from the NICA and optimized Multiview analysis (Table 2) into binary indices (0s & 1s) by rounding, so that weak correlations (<0.5) are assigned a value of 0, and stronger ones (≥ 0.5) are assigned a value of 1. This yielded a group permutation with repetition for each bundle's correlation results, following the sample arrangement in the heatmap figure (Figure 6a-c). This evaluation identified some fake notes, though some remain unclassified as the count of genuine (1s) exceeded the actual number of genuine notes in the bundle. This discrepancy arose because some fake notes show significant similarity to the genuine note, leading to an overestimation of genuine notes or underestimation of fake notes below the 0.5 threshold.

To selectively filter out weaker matches and ensure a more precise identification of genuine notes among those identified as likely genuine (1s), we defined a dynamic threshold in Equation 12. A correlation with a deviation from the absolute correlation of the genuine note exceeding the dynamic threshold, suggests a higher likelihood of forgery and was transformed to 0; otherwise, it was transformed to 1. The filtered results of the Multiview NICA and optimized Multiview spectral sets formed new group permutations for the optimized correlation (Figs. 7a & b, 8a & b, and 9a & b) respectively.

Genuine similarity = deviation
<= dynamic threshold 12

Where

deviation = 1 – correlation 13

dynamic threshold = mean of deviation – K × standard deviation, and K = 1.

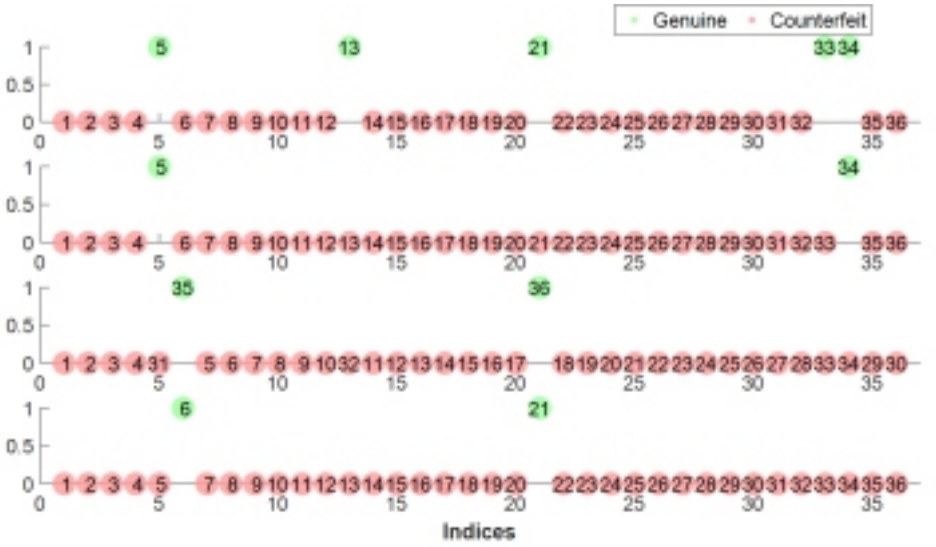

Figure 7. Bundle C. a) Mv-NICA permutation. b) Optimize Multiview Permutation. c) Permutation product of a and b given the sample spatial localization in the bundle. d) Bundle arrangement based on Table 2. Green dots represent Genuine notes, red dots represent Counterfeit notes.

Figure 8. Bundle D. a) Mv-NICA permutation. b) Optimize Multiview Permutation. c) Permutation product of a and b given the sample spatial localization in the bundle. d) Bundle arrangement based on Table 2. Green dots represent Genuine notes, red dots represent Counterfeit notes

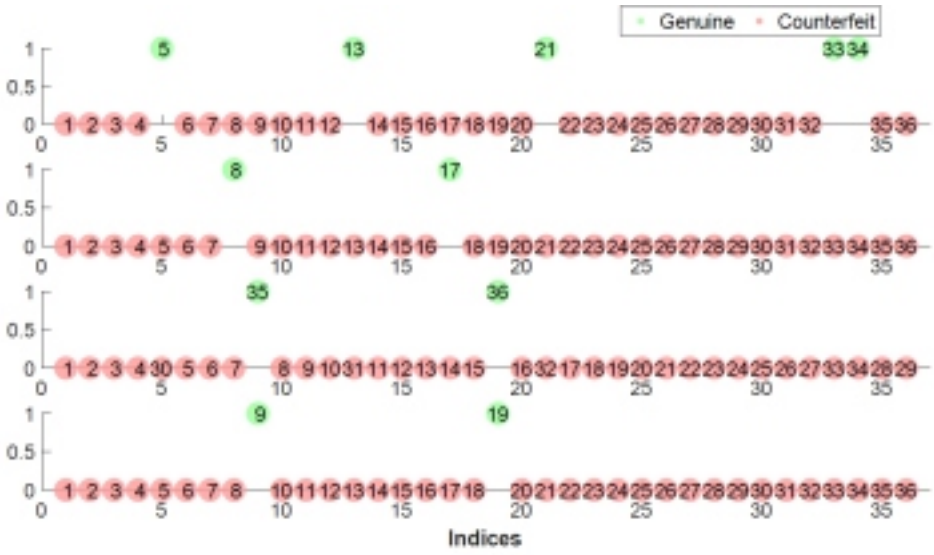

Figure 9. Bundle E a) Mv-NICA permutation. b) Optimize Multiview Permutation. c) Permutation product of a and b given the sample spatial localization in the bundle. d) Bundle arrangement based on Table 2. Green dots represent Genuine notes, red dots represent Counterfeit notes

Permutation-Based Localization of Multiview Spectra Set of Notes in a Bundle

Two groups of permutations with repetition were obtained from the Genuine similarity (Equation 12) of the Multiview NICA and the optimized Multiview spectra data sets for each bundle's content. A permutation product analysis was conducted on these datasets to identify the spatial localization of individual notes within the actual bundle. A permutation product between the group permutation of the Multiview-transformed correlation result on the left (outer permutation) and the group permutation of the Mv-NICA-transformed correlation result on the right (inner permutation) was evaluated, following the procedure in Table 3. Figures 7c, 8c and 9c present the permutation products, while Figures 7d, 8d, and 9d show the actual sample localization in the bundle's front view (Table 1). Therefore, all genuine samples in each bundle are correctly localized (compare Figures 7c & 7d, 8c & 8d, and 9c & 9d), confirming that all counterfeit notes are also detected and localized.

CONCLUSION

We successfully demonstrated a robust Multiview Raman spectroscopy technique for the simultaneous authentication of multiple counterfeit ₦500 and ₦1000 notes (and multiple genuine notes also) in a bundle in situ. The research highlights that Raman spectroscopy can detect subtle differences in the substrate molecular composition of genuine and counterfeit notes, even when they exhibit similar spectral profiles. Extracting the individual spectra of notes from the Mv-composite data alone does not allow for the identification of individual notes and their spatial localization in the bundle. A combination of two-dimensional correlation analysis and permutation-based localization of the Multiview spectral signatures identifies both genuine and counterfeit notes along with their localization in the bundle in situ.

Our approach overcomes the traditional limitations of Raman spectroscopy, which typically identifies only single notes per analysis. Instead, it offers simultaneous analysis, detection, and localization of multiple genuine and counterfeit notes in a bundle in situ, with applications in forensic document spectroscopy. Our findings will contribute significantly to the efforts of legal institutions, intelligence organizations, and financial authorities in anti-counterfeiting, significantly reducing counterfeiting risk and increasing trust in financial transactions.

Future research can adapt this approach to other currencies and security documents around the world and also explore advanced machine learning algorithms to extract more features in the data.

ACKNOWLEDGEMENTS
The authors thanks Electron Microscope Unit, University of Cape Town, Rondebosch, 7700 South Africa and Miranda's team for their support and expertise.

FUNDING
none

CONFLICT OF INTEREST
The authors declare no conflict of interest

AUTHORS CONTRIBUTION
A.M.K.: Conceptualization, Methodology, Software-Programming Validation, Formal Analysis, Resources, Data-Curation, Writing-Original Draft, Writing-Review & Editing, Visualization, Project Administration, Funding. **A.M.H.** : Supervision, Guidance.

REFERENCES

Agarwal, U. P. 2019. Analysis of Cellulose and Lignocellulose Materials by Raman Spectroscopy: A Review of the Current Status. *Molecules*, 24: 1659. doi: 10.3390/molecules24091659

Ali, K. (9 June, 2023). Turkey Seize $1 Billion of counterfeit Money Headed for Africa. *Reuters*. https://www.reuters.com/world/turkey-seizes-1-bln-counterfeit-money-headed-africa-2023-06-09/

Bitla, S. 2002. Application of Raman Techniques for Paper Coatings Application of Raman Techniques. (Master of Science dessertation) The University of Maine. Orono USA. DigitalCommons@UMaine. (1-69.). http://digitalcommons.library.umaine.edu/etd/236

Boyd, S., & Vandenberghe, L. 2006. Convex Optimization (N. Anna, Nicholas & D. and Margriet (eds.); 2009th ed., Vol. 3, Issue 1). Cambridge University Press. https://web.stanford.edu/~boyd/cvxbook/bv_cvxbook.pdf

Brandão, J. M. D. O. B., Almeida, N. S. M., Dixini, P. V. M., Baier, C. H. A., Dias, H. P., Bassane, J. F. P., França, H. S., Silva, S. R. C., Aquije, G. M. F. V., & Romão, W. 2016. Documentoscopy by atomic force microscopy (AFM) coupled with Raman microspectroscopy: Applications in banknote and driver license analyses. *Analytical Methods*, 8(4): 771-784. doi:10.1039/c5ay03128a

Brigitta, N., Attila F., Enik? B., Panna V., Zsombor K. N., and György M. 2018. Raman Spectroscopy for Process Analytical Technologies of Pharmaceutical Secondary Manufacturing. *American Association of Pharmaceutical Scientists*. (20), (1). doi:10.1208/s12249-018-1201-2

Cheng, D., Shi, Z., Tan, X., Zhu, Z., Jiang, Z., & Nmf, A. 2010. A Method of Automatically Estimating the Regularization Parameter for Non-negative Matrix Factorization. Sixth International Conference on Natural Computation (ICNC), 22-26. doi:10.1109/icnc.2010.5583822

Cody, W. C, Charles D., Nicholas B. R., Daniel R., Emily E. A., Kyle S. Mohammad A. A., Julian R. Vilayanur S. R. and Darren J. L 2017. Human Ability to Discriminate Surface Chemistry by Touch. *The Royal Society of Chemistry*. (5) 70-77. doi:10.1039/c7mh00800g

Daniel, D. L. and Seung, S. 1999. Learning the parts of objects by non-negative matrix factorization. *Nature*, 401(6755): 788-791. doi:10.1038/44565

Dikbaş, F. 2017. A novel two-dimensional correlation coefficient for assessing associations in time series data. *International Journal of Climatology*, 37(11): 4065-4076. doi:10.1002/joc.4998

Donatus, A., 2023. Counterfeit Naira Banknotes in Circulation, CBN Alearts Nigerians. Channels Television. https://www.channelstv.com/2023/12/08/counterfeit-naira-banknotes-in-circulation-cbn-alerts-nigerians/

Gegenfurtner, K. R. 2003. Cortical Mechanisms of Colour Vision. Nature Review. 4: 563-572.
doi:10.1038/nrn1138

Gierlinger, N., Luss, S., König, C., Konnerth, J., Eder, M., & Fratzl, P. 2010. Cellulose microfibril orientation of Picea abies and its variability at the micron-level determined by Raman imaging. *Journal of Experimental Botany*, 61(2): 587-595.
doi:10.1093/jxb/erp325

Gordon, K. C., & Mcgoverin, C. M. 2011. Raman mapping of pharmaceuticals. *International Journal of Pharmaceutics*, 417(1-2): 151-162.
doi:10.1016/j.ijpharm.2010.12.030

Guedes, A., Algarra, M., Prieto, A. C., Valentim, B., Hortelano, V., Neto, S., Algarra, R., & Noronha, F. (2013). Raman microspectroscopy of genuine and fake euro banknotes. *Spectroscopy Letters*, 46(8): 569-576.
doi:10.1080/00387010.2013.769007

Hana, V., P. T. and M. S. 2019. Application of Raman Spectroscopic Measurement for Banknote Security Purposes (P. B. and A. C. Klimis Ntalianis, George Vachtsevanos (ed.); pp. 42-47).
doi:10.1007/978-3-030-21507-1_7

He, P., Bitla, S., Bousfield, D., and Tripp, C. P. 2002. Raman Spectroscopic Analysis of Paper Coatings. in Applied Spectroscopy (vol. 56, issue 9).
doi:10.1366/000370202760295322

James, H. W and Rajai, H. A. 1987. Raman spectra of celluloses. The Institute of Paper Chemistry, Appleton, Wisconsin IPC Technical Paper Series Number 226

Jauković, G. 2019. Advantages and Disadvantages of Raman Spectroscopy in Testing Paper. *Technical Journal*, 3(3): 226-229.
doi:10.31803/tg-20190328155758

Jerome J. and Workman, Jr. (2001). Infrared and Raman spectroscopy in paper and pulp analysis. Applied Spectroscopy Reviews, 36(2–3), 139–168.
doi: 10.1081/ASR-100106154

Jing, W. 2017. Advances in Nonnegative Matrix Factorization with Application on Data Clustering. (Doctoral dissertation, Bournemouth University).
https://eprints.bourmemouth.ac.uk/30354/

Kylie, J., Sarah, B. and Claude, R. 2013. The forensic analysis of office paper using carbon isotope ratio mass spectrometry. Part 3: Characterizing the source materials and the effect of production and usage on the δ^{13} C values of paper, *Forensic Science International* 233: 355-364.
doi:10.1016/j.forsciint.2013.10.011

Lawandy, N. M., & Smuk, A. Y. (2014). Supercritical Fluid Cleaning of Banknotes. *Industrial and Engineering Chemistry Research,* 53(2): 530-540.
doi: 10.1021/ie403307y

Lee, H. and S. C. 2009. Group Nonnegative Matrix Factorization for EEG Classification. Proceedings of the 12th International Conference on Artificial Intelligence and Statistics (AISTATS), Clearwater Beach, Florida, USA, 5, 320-327.

Linder, T., & Lofqvist, T. 2012. Anisotropic light propagation in paper. *Nordic Pulp and Paper Research*, 27(2): 500-505.
doi:10.3183/npprj-2012-27-02-p500-506

Luo, J., Xie, J., & Fan, W. 2014. Study on Identification of 100 % Cotton Fabric by Raman Spectroscopy and Random Forest. *Advanced Materials Research*, (1033-1034): 439-443.
doi:10.4028/www.scientific.net/AMR.1033-1034.439

Marabello, D., Benzi, P., Lombardozzi, A., & Strano, M. 2017. X-ray Powder Diffraction for Characterization of RaFw Materials in Banknotes. *Journal of Forensic Sciences*, 62(4): 962-970.
doi:10.1111/1556-4029.13392

Miron, S., Dossot, M., Carteret, C., Margueron, S., & Brie, D. 2011. Join Processing of the Parallel and Cross Polarized Raman Spectra and Uniqueness in Blind Nonnegative Source Separation. *Chemometrics and Intelligent Laboratory Systems*, 105: 7-18.
doi: 10.1016/j.chemolab.2010.10.005

Pedersen, M. S. 2012. The Matrix Cookbook. http://matrixcookbook.com

Pelletier, M. J. 2003. Quantitative Analysis Using Raman Spectrometry. *Focal Point*, 57: 20A-42A.
doi:10.1366/000370203321165133

Peter Weiderer, A. M. T. & E. W. L. 2019. Decomposing Temperature Time Series with Non-Negative Matrix Factorization. arXiv:1904.02217v1. 1-12.

Ruchita, S. D. and Agrawal, Y. K. 2021. Raman Spectroscopy: Recent Advancements, Techniques and Applications, *Vibrational Spectroscopy*. 57; 163- 176. doi: 10.1016/j.vibspec.2011.08.003

Shahdan, P. 1961. Permutation Ordering and Identification. *Mathematics Magazine*, 34(6): 353-358. doi:10.1080/0025570X.1961.11975264

Takalo, J., Timonen, J., Sampo, J., Rantala, M., Siltanen, S., & Lassas, M. 2014. Using the fibre structure of paper to determine authenticity of the documents: Analysis of transmitted light images of stamps and banknotes. *Forensic Science International*, 244: 252-258. doi:10.1016/j.forsciint.2014.09.002

Tian, Y., & Zhang, Y. 2022. A comprehensive survey on regularization strategies in machine learning. *Information Fusion*, 80(October 2021), 146-166. doi:10.1016/j.inffus.2021.11.005

Vaskova, H., & Valasek, P. 2016. Authentication of Czech Banknotes using Raman Microscopy. The Tenth International Conference on Emerging Security Information, Systems and Technologies; pp 220-224.

Wang, J., Tian, F., Wang, X., Yu, H., Liu, C. H., & Yang, L. 2012. Proceedings of the Twenty-Sixth International Joint Conference on Artificial Intelligence Main track. Pp 2922-2928. doi:10.24963/ijcai.2017/407

Was-Gubala, J., & Machnowski, W. 2014. Application of Raman Spectroscopy for Differentiation Among Cotton and Viscose Fibers Dyed with Several Dye Classes Application of Raman Spectroscopy for Differentiation Among Cotton and Viscose Fibers Dyed with Several Dye Classes. 7010 (January 2016). doi:10.1080/00387010.2013.820760

Yang, Y. and Wang H, 2018. Multi-view clustering: A survey. in Big Data Mining and Analytics, 1(2): 83-107. doi:10.26599/BDMA.2018.9020003

Yu-Xiong, Wang and Yu-Jin, Zhang 2013. Nonnegative Matrix Factorization: A Comprehensive Review. in IEEE Transactions on Knowledge and Data Engineering, vol. 25, no. 6, pp. 1336-1353, June 2013. doi:10.1109/TKDE.2012.51